Journal of Magnetism and Magnetic Materials 324 (2012) 610–615

Contents lists available at SciVerse ScienceDirect

Journal of Magnetism and Magnetic Materials

journal homepage: www.elsevier.com/locate/jmmm

Temperature-dependent Heisenberg exchange coupling constants from linking electronic-structure calculations and Monte Carlo simulations

D. Böttcher [a,b], A. Ernst [a], J. Henk [a,*]

[a] Max-Planck-Institut für Mikrostrukturphysik, Weinberg 2, D-06120 Halle (Saale), Germany
[b] Institut für Physik, Martin-Luther-Universität Halle-Wittenberg, Von-Seckendorff-Platz 1, D-06120 Halle (Saale), Germany

ARTICLE INFO

Article history:
Received 12 July 2011
Received in revised form
19 August 2011
Available online 8 September 2011

Keywords:
Classical spin models
Exchange coupling
Numerical simulations
Electronic-structure calculations

ABSTRACT

We propose a method to calculate the temperature dependence of Heisenberg exchange coupling constants J_{ij}. Within the formalism of disordered local moments (DLM), the magnetization and the J_{ij} are computed from first principles for any concentration c of the magnetic constituents. The exchange coupling constants are then used in Monte Carlo (MC) simulations to compute the temperature dependence of the magnetization for the given c. By comparing the magnetization from DLM calculations and from MC simulations we obtain a mapping of temperature versus concentration and eventually temperature-dependent J_{ij}. The approach which is applied to bulk Fe and Co can for example improve critical exponents.

1. Motivation

The classical Heisenberg model is widely used to describe ground-state properties and phase transitions in magnetic systems. In particular critical temperatures T_c, critical exponents, and magnetization curves $\langle m\rangle(T)$ can be calculated. It is also part of atomistic magnetization dynamics simulations within the framework of the Landau–Lifshitz–Gilbert equation (e.g. Refs. [1,2]).

An exchange coupling constant J_{ij} in the classical Heisenberg model, whose Hamiltonian reads

$$H = -\sum_{ij} J_{ij}\hat{m}_i \cdot \hat{m}_j, \tag{1}$$

quantifies the energy change upon rotating the local magnetic moments (unit vectors) $\hat{m}_i$ at site i and $\hat{m}_j$ at site j. The J_{ij} are taken either as adjustable parameters or are computed from first principles.

First-principles electronic-structure calculations are usually performed for zero temperature. The set $\{J_{ij}\}$ of exchange coupling constants is obtained from the energy change of tilting local magnetic moments or from a Kubo-Greenwood-type expression of Green functions [3]. From these J_{ij}, critical temperatures can be calculated within the mean-field approximation or the random-phase approximation; or they are used in simulations, for example in Monte Carlo simulations. In any case, the J_{ij} are computed for $T = 0$ K but are taken to describe systems at finite temperatures.

In contrast to the preceding, the disordered local moment (DLM) picture [4–6] describes paramagnetic systems, that is at temperatures $T \geq T_c$. Within the DLM approach, nonzero local magnetic moments are maintained but the directions of these fluctuate so strongly that the average magnetization vanishes. In their simplest form, the thermal fluctuations are modeled by a substitutional Ising-type alloy whose constituents $\Uparrow$ and $\Downarrow$ are oppositely magnetized atoms (local moment orientations $\hat{m}_\Uparrow = -\hat{m}_\Downarrow$). At alloy concentration $c_\Uparrow = 1 - c_\Downarrow = 0.5$, that is at T_c, the two local moments cancel although $m_\Uparrow$ and $m_\Downarrow$ are nonzero; this in contrast to the Stoner model in which the magnetization vanishes everywhere in space at T_c (i.e. $m_\Uparrow = m_\Downarrow = 0$). In first-principles calculations, the DLM approach can be treated within the coherent potential approximation (CPA) [7] from which the set $\{J_{ij}\}$ can be computed as well.

With respect to the preceding, we are concerned with two different sets of exchange constants: $\{J_{ij}(0)\}$ and $\{J_{ij}(T_c)\}$. This suggests the problem whether one can obtain sets $\{J_{ij}(T)\}$ for *every* temperature between 0 K and T_c. Since in the CPA modeling of the DLM approach $c_\Uparrow = 1$ would be equivalent to $T = 0$ K and $c_\Uparrow = 0.5$ to $T = T_c$, the task is to map the entire concentration range [0.5, 1.0] onto the temperature range [0 K, T_c]. However, there is no direct relation $c_\Uparrow \leftrightarrow T$ within the DLM approach itself; consequently the mapping $T(c_\Uparrow)$ requires an additional ingredient which in this work is the classical Heisenberg model.

In this paper, we propose a simple way to obtain sets $\{J_{ij}(T)\}$ as follows. The exchange parameters are computed from first principles within the DLM approach at a concentration $c_\Uparrow$. This set $\{J_{ij}(c_\Uparrow)\}$ is then used in Monte Carlo (MC) simulations of the classical Heisenberg model at a temperature T. The requirement

* Corresponding author.
E-mail address: henk@mpi-halle.de (J. Henk).

0304-8853/$ - see front matter © 2011 Elsevier B.V. All rights reserved.
doi:10.1016/j.jmmm.2011.08.053

that the average magnetization $\langle m\rangle(c_\Uparrow)$ in the DLM calculations and $\langle m\rangle(T;c_\Uparrow)$ in the MC simulations are equal yields the mapping $T(c_\Uparrow)$. We apply this approach to bulk Fe and Co. Problems and improvements are discussed as well.

Before introducing the approach a few notes on other first-principles approaches to the temperature dependence of magnetism are in order. Pindor et al. [7] used the DLM formalism as well but the temperature dependence was restricted to the self-consistent electronic-structure calculation, in the spirit of the finite-temperature version of spin-density functional theory. The magnetic fluctuations were modeled by a paramagnetic Ising-type alloy (with concentration 50%, treated within the CPA). A two-step approach to the temperature dependence was introduced by Ruban et al. [8]. There, the exchange interaction constants were determined from constrained local spin-density approximation calculations and subsequently used in a model Hamiltonian to investigate finite-temperature magnetic properties. Drchal et al. investigated the joint effect of temperature and disorder on the interlayer exchange coupling [9]. There, the temperature entered the exchange coupling energy via the Fermi–Dirac distribution; magnetic fluctuations were not considered.

Using a relativistic DLM approach, Buruzs [10] studied temperature-dependent properties of thin films. This approach is computationally demanding because it involves both rotational averaging over the magnetic-moment directions and the computation of Weiss fields. Since each local Weiss field is aligned along the average magnetization, the magnetization curve is given by a Langevin function. Although not done in Ref. [10], this formalism allows to calculate the temperature dependencies of both Heisenberg exchange-coupling constants and Dzyaloshinskii–Moriya vectors. In the present approach which uses the computationally less demanding Ising-type averaging, the temperature-concentration mapping is lost but is reintroduced by comparison with Heisenberg Monte Carlo simulations. In the latter, the local Weiss fields are determined by the local magnetic moments within the finite range of exchange interactions. As a consequence, the magnetization curve is no longer a Langevin function and critical exponents can be improved.

The paper is organized as follows. Computational aspects of the proposed approach are given in Section 2. Its applications to Fe (3.1) and Co (3.2) are presented and discussed in Section 3. Conclusions and a brief outlook are given in Section 4.

2. Computational aspects

The Heisenberg exchange coupling constants J_{ij} of bulk bcc Fe and hcp Co are calculated from first principles using a scalar-relativistic multiple-scattering approach (KKR, Korringa–Kohn–Rostoker method [11]), with the exchange-correlation functional taken from Ref. [12].

For sites $i\neq j$, the exchange coupling constants are given by [3]

$$J_{ij}=\frac{1}{4\pi}\mathrm{tr}\int^{E_\mathrm{F}}\Delta \mathrm{t}_i\tau_{ij}^{\uparrow}\Delta \mathrm{t}_j\tau_{ji}^{\downarrow}\,\mathrm{d}E, \tag{2}$$

with $\Delta \mathrm{t}_i\equiv \mathrm{t}_i^{\uparrow}-\mathrm{t}_i^{\downarrow}$. t_i^{σ} and τ_{ij}^{σ} are the spin-resolved KKR single-site scattering matrices and the scattering-path matrices in spin-angular-momentum representation ($\sigma=\uparrow,\downarrow$) [11]. τ_{ij} describes the propagation of an electron from site j to site i. The energy integral runs up to the Fermi energy E_F.

The ferromagnet at temperature T is described as a substitutional binary alloy within the coherent potential approximation (CPA) [13–16]. Each site is occupied by an atom magnetized along the z direction ($\Uparrow$) with concentration $c_\Uparrow$ and an atom magnetized along the $-z$ direction ($\Downarrow$) with concentration $c_\Downarrow=1-c_\Uparrow$; local moment orientations are denoted by $\Uparrow$ and $\Downarrow$ while spin orientations are denoted by $\uparrow$ and $\downarrow$. At $c_\Uparrow=1$ the sample is perfectly magnetically ordered, which corresponds to $T=0$ K. At $c_\Uparrow=0.5$ it is paramagnetic, which corresponds to $T=T_\mathrm{c}$. Within the KKR-CPA approach used in this paper, short-range order is neglected.

The $\Uparrow$ and $\Downarrow$ atoms are created at site i in the effective CPA medium by defect matrices $\mathrm{D}_{i\mu}$ ($\mu=\Uparrow,\Downarrow$) [11]. The effective CPA medium is described by scattering-path matrices τ_{ij}^{cpa}. More precisely, a defect of type μ at site i and a defect of type ν at site j are introduced by replacing τ_{ij} by $\tilde{\tau}_{i\mu,j\nu}\equiv \mathrm{D}_{i\mu}\tau_{ij}^{\mathrm{cpa}}\mathrm{D}_{j\nu}$. Without vertex corrections, that is by approximating the configurational average of the product of scattering-path matrices in Eq. (2) by a product of the individual configurational averages, we have

$$J_{i\mu,j\nu}=\frac{c_\mu c_\nu}{4\pi}\mathrm{tr}\int^{E_\mathrm{F}}\Delta \mathrm{t}_{i\mu}\tilde{\tau}_{i\mu,j\nu}^{\uparrow}\Delta \mathrm{t}_{j\nu}\tilde{\tau}_{j\nu,i\mu}^{\downarrow}\,\mathrm{d}E,\quad \mu,\nu=\Uparrow,\Downarrow. \tag{3}$$

Since the CPA equations are solved self-consistently at each energy E, this approach is beyond a rigid-band model.

We define effective exchange coupling constants

$$J_{ij}^{\mathrm{eff}}\equiv J_{i\Uparrow,j\Uparrow}-J_{i\Uparrow,j\Downarrow}-J_{i\Downarrow,j\Uparrow}+J_{i\Downarrow,j\Downarrow}. \tag{4}$$

A positive (negative) $J_{i\mu,j\nu}$ favors parallel (antiparallel) alignment of the local moments ($J_{i\Uparrow,j\Downarrow}=J_{i\Downarrow,j\Uparrow}$). As a result, $J_{i\Uparrow,j\Downarrow}$ and $J_{i\Downarrow,j\Uparrow}$ appear with a minus sign in Eq. (4). The set of $\{J_{ij}^{\mathrm{eff}}\}$ enters the classical Heisenberg model, Eq. (1), which is solved by Monte Carlo simulations [17,18].

The mapping $T(c_\Uparrow)$ of the concentration $c_\Uparrow$ on the temperature T is obtained via the average magnetization $\langle m\rangle$ which can be computed from the Heisenberg MC simulations and the first-principles DLM calculations. First, we choose a concentration $c_\Uparrow=1-c_\Downarrow$ and compute within the DLM picture $\langle m\rangle(c_\Uparrow)$ and the set $\{J_{ij}(c_\Uparrow)\}$. This set is then used in the Heisenberg MC simulations in which the temperature T is scanned, yielding the magnetization curve $\langle m\rangle(T;c_\Uparrow)$. The requirement $\langle m\rangle(T;c_\Uparrow)=\langle m\rangle(c_\Uparrow)$ fixes T for the chosen $c_\Uparrow$, which yields eventually the mapping $T(c_\Uparrow)$.

3. Results and discussion

3.1. Fe

3.1.1. Electronic structure and magnetization

The concentration dependence of the exchange coupling constants is completely determined by those of the scattering-path matrices $\tilde{\tau}_{j\nu,i\mu}^{\sigma}$ and of the single-site scattering matrices $\Delta \mathrm{t}_{i\mu}$ in Eq. (3). Hence, we first address the electronic structure by means of the density of states (DOS; Fig. 1).

The d-majority states for ferromagnetic Fe are almost completely occupied [cf. the shoulder at E_F for $c_\Uparrow=1$ in Fig. 1(a)]. These states become depopulated with decreasing $c_\Uparrow$ so that at $c_\Uparrow=0.5$ the sample is nonmagnetic. For $c_\Uparrow=1$ the DOS is strongly textured, which indicates an ordered configuration; for smaller concentrations, the DOS is smeared out, as is typical for a disordered configuration. Similar densities of states were found by averaging over random local-moment configurations with mean-field distribution [19].

The trends in the total DOS show also up in the impurity DOS [Fig. 1(b) and (c)]. Note that for $c_\Uparrow=1$ the $\Uparrow$-DOS is identical to the total DOS in (a). Further for $c_\Uparrow=0.5$ the host is nonmagnetic and consequently the spin-$\uparrow$ DOS of an $\Uparrow$ impurity is the same as spin-$\downarrow$ DOS of a $\Downarrow$ impurity. An analogous relation holds for the opposite spin projection.

In the Stoner picture, the magnetization vanishes for a paramagnetic sample everywhere in space. In the DLM picture, however, the host magnetization $\langle m\rangle=c_\Uparrow m_\Uparrow+c_\Downarrow m_\Downarrow$ vanishes but the impurity magnetizations $m_\Uparrow$ and $m_\Downarrow$ themselves remain finite [Fig. 2(a)]. More precisely, $m_\Uparrow=-m_\Downarrow$ for $c_\Uparrow=0.5$; they are, in absolute value, as large as the magnetization of ferromagnetic

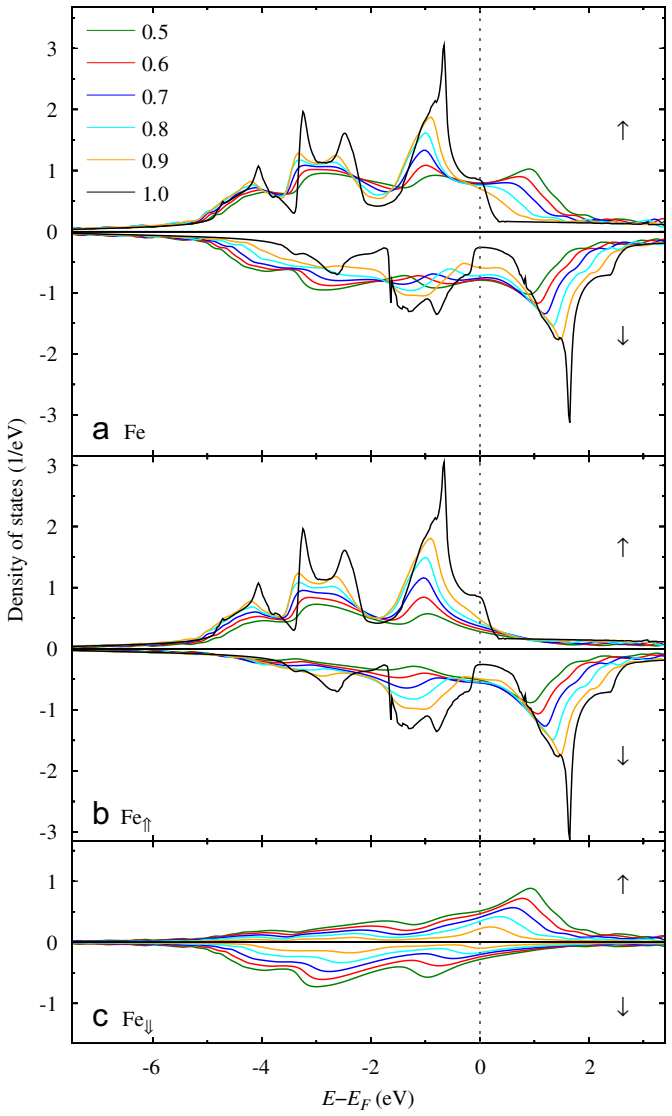

Fig. 1. Spin-resolved electronic structure of bulk Fe. (a) The total density of states (DOS) is shown for different concentrations $c_{\Uparrow}$, as indicated (majority spin ↑, minority spin ↓). (b) Density of states for an ⇑ impurity in the effective CPA medium, weighted by the concentration $c_{\Uparrow}$. (c) As (b) but for a ⇓ impurity. The Fermi energy is E_F.

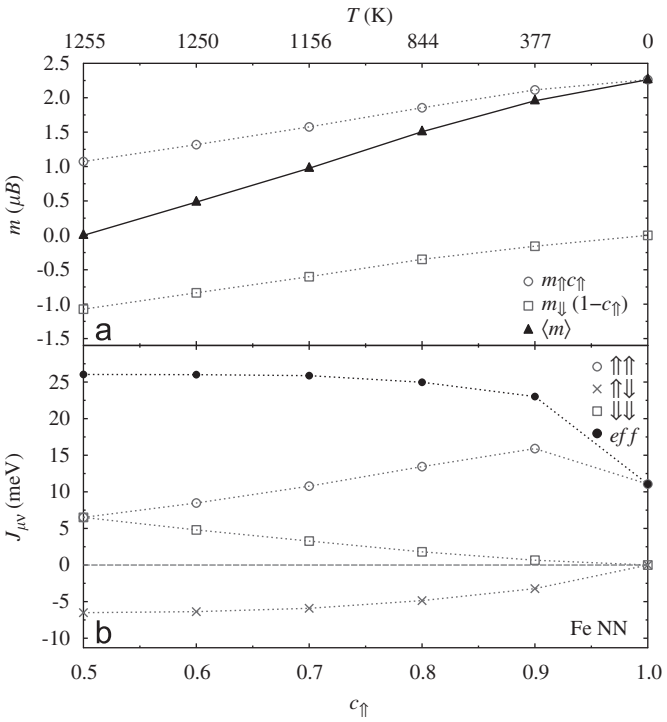

Fig. 2. Magnetization and exchange coupling in bulk Fe. (a) The concentration-weighted impurity magnetizations $c_{\Uparrow}m_{\Uparrow}$ (circles) and $c_{\Downarrow}m_{\Downarrow}$ (squares) are displayed versus concentration $c_{\Uparrow}=1-c_{\Downarrow}$. The average magnetization $\langle m\rangle = c_{\Uparrow}m_{\Uparrow}+c_{\Downarrow}m_{\Downarrow}$ (triangles) is shown in addition. (b) Nearest-neighbor exchange coupling constants $J_{\Uparrow\Uparrow}$ (empty circles), $J_{\Uparrow\Downarrow}$ (crosses), $J_{\Downarrow\Downarrow}$ (empty squares) are depicted versus concentration $c_{\Uparrow}$. The effective constant $J_{\rm eff}$ (filled circles) decreases with $c_{\Uparrow}$. The temperature scale at the top axis refers to the $T\leftrightarrow c_{\Uparrow}$ mapping shown in Fig. 5. Lines serve as guides to the eye.

bcc-Fe (2.26 μ_B at $T=0$ K) so that the concentration-weighted moments $c_{\Uparrow}m_{\Uparrow}$ and $c_{\Downarrow}m_{\Downarrow}$ depend almost linearly on their concentration. Consequently, $\langle m\rangle$ depends to a very good approximation linearly on $c_{\Uparrow}$ as well.

3.1.2. Heisenberg exchange coupling constants

As an example, we address the concentration dependence of the nearest-neighbor exchange coupling constants [Fig. 2(b)]. For $c_{\Uparrow}=0.5$ the host is nonmagnetic, that is $(\tau_{ij}^{\rm cpa})^{\uparrow}=(\tau_{ij}^{\rm cpa})^{\downarrow}$ in Eq. (3); therefore $J_{\Uparrow\Uparrow}=J_{\Downarrow\Downarrow}=-J_{\Uparrow\Downarrow}=-J_{\Downarrow\Uparrow}$. As a consequence of the decreasing (in absolute value) $J_{\Downarrow\Downarrow}$, $J_{\Uparrow\Downarrow}$, and $J_{\Downarrow\Uparrow}$ with $c_{\Uparrow}$, the effective exchange coupling constant $J_{\rm eff}$ decreases monotonously, which implies a smaller critical temperature T_c for $c_{\Uparrow}=1$ than for 0.5.

$J_{\rm eff}$ shows a rapid drop close to $c_{\Uparrow}=1$ which is due to the contribution of $J_{\Uparrow\Uparrow}$. This decay may be related to the spin-resolved DOS of an ⇑ impurity in the energy range close to E_F [Fig. 1(b)]. The energies around E_F are important because the electronic structure at these energies determine essentially the electron propagation. The densities of states of both spin projections are almost constant for small $c_{\Uparrow}$. But both show 'jumps' from $c_{\Uparrow}=0.9$ to 1.0. These 'jumps' may be the reason for the fast decrease of $J_{\Uparrow\Uparrow}$ in that concentration range. Please be aware that this argument is by no means strict but handwaving.

The nearest-neighbor exchange constant for $c_{\Uparrow}=1$ compares well with data from the literature; cf. for example Refs. [20–22]. While the $J_{i\Uparrow,j\Uparrow}$ oscillate with distance $d_{ij}\equiv|\vec{r}_i-\vec{r}_j|$ [Fig. 3(a)], in particular for $c_{\Uparrow}=1$ (asterisks), the exchange constants $J_{i\Uparrow,j\Downarrow}$ (b) and $J_{i\Downarrow,j\Downarrow}$ (c) are sizable only for nearest neighbors ($d_{ij}=4.69$ Bohr). This implies that at small $c_{\Uparrow}$, or close to T_c, the local Weiss fields in the Heisenberg model are given mainly by the average magnetization of the nearest-neighbor shells. At $c_{\Uparrow}$ close to 1, or at low temperatures, the Weiss fields are determined in a larger interaction range. As a consequence, the magnetization curves $\langle m\rangle(T;c_{\Uparrow})$ show different critical exponents, as we will discuss in Section 3.1.3.

3.1.3. Critical temperature and temperature-concentration mapping

As motivated in the preceding subsection, the critical temperature T_c decreases with concentration, as is fully confirmed by the Monte Carlo simulations (Fig. 4). The nonzero magnetizations $\langle m\rangle(T;c_{\Uparrow})$ for $T>T_c$ that are typical for finite systems do not allow a precise determination of T_c. Hence, the T_c's were obtained from MC simulations with various system sizes using Binder's fourth cummulant U_4 (Refs. [18,23]; 3180 sites were used for Fig. 4).

For concentrations $c_{\Uparrow}$ up to 0.7, T_c is almost constant and then decays smoothly [filled circles in Fig. 5(a)]. This finding is in line with the concentration dependence of the nearest-neighbor

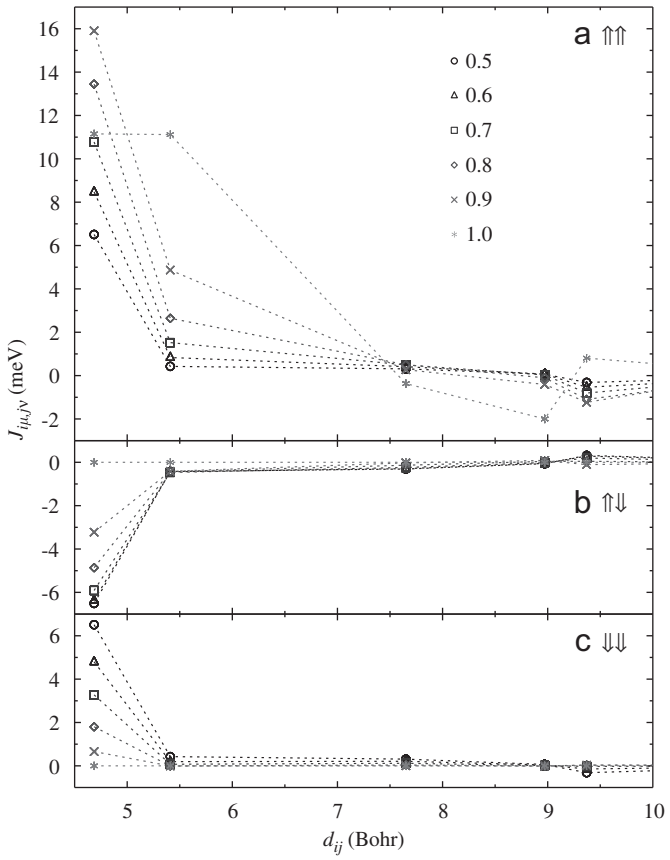

Fig. 3. Distance dependence of the exchange coupling constants in bulk Fe. The exchange constants $J_{i\mu,j\nu}$, defined in Eq. (3), are shown versus distance $d_{ij} \equiv |\vec{r}_i - \vec{r}_j|$ for (a) $\mu = \nu = \Uparrow$, (b) $\mu = \Uparrow$, $\nu = \Downarrow$, and (c) $\mu = \nu = \Downarrow$. The symbols represent different concentrations $c_{\Uparrow} = 1 - c_{\Downarrow}$, as indicated in (a). Lines serve as guides to the eye.

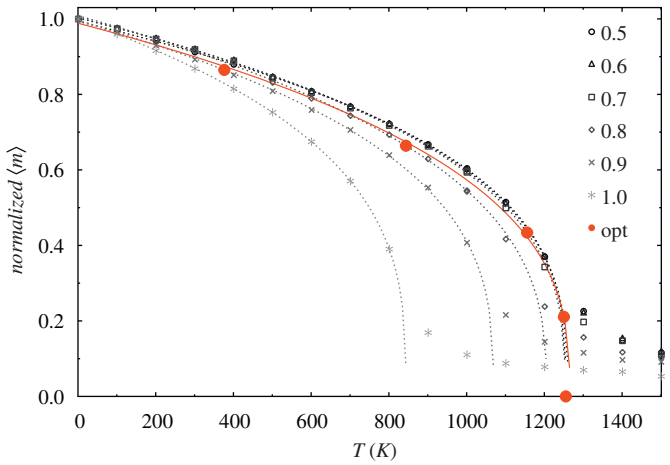

Fig. 4. Magnetization-temperature curves $\langle m \rangle(T; c_{\Uparrow})$ for bulk Fe, as obtained from Monte Carlo simulations and normalized to $\langle m \rangle$ for $T = 0$ K. Curves for different concentrations $c_{\Uparrow}$ are distinguished by symbols, as indicated. The magnetization curve using the temperature-concentration mapping from Fig. 5 is shown in addition ('opt', large filled circles). Each magnetization curve has been approximated by $\langle m \rangle \propto (T_c - T)^{\beta}$, with fixed T_c (dotted lines).

exchange coupling constants [Fig. 2(b)]. For $c_{\Uparrow} = 1$, the T_c of 844 K is smaller than the experimental value (1045 K) while for $c_{\Uparrow} = 0.5$ it is larger (1255 K; a similar mismatch was found by Buruzs [10]). The same holds for T_c from the mean-field approximation (1002 K and 1731 K, respectively) but the covered temperature range is much larger than that in the MC calculations.

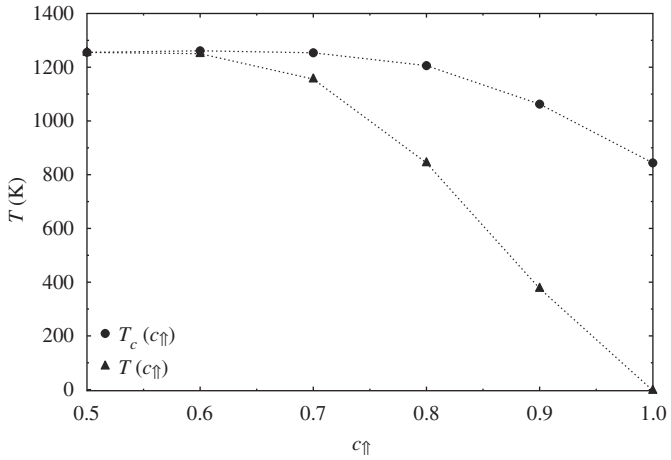

Fig. 5. Critical temperature and temperature-concentration mapping of bulk Fe. T_c is displayed versus concentration $c_{\Uparrow}$ (filled circles), while the temperature-concentration mapping $T(c_{\Uparrow})$ is displayed by filled triangles. $\partial T/\partial c_{\Uparrow} = \partial T_c/\partial c_{\Uparrow} = 0$ at $c_{\Uparrow} = 0.5$. Lines serve as guides to the eye.

The mismatch of the T_c obtained from the MC simulations and the experimental values may be explained as follows. While the DLM calculation for $c_{\Uparrow} = 0.5$ mimics a random configuration and the calculation for $c_{\Uparrow} = 1$ mimics the perfectly ordered configuration, it is conceivable that the best description is obtained by a disordered configuration with short-range order [24,25]. Short-range order can be accounted for within the non-local CPA, the embedded-cluster CPA [26] or the locally self-consistent Green function method [27]. Other reasons might be that the present DLM calculations use an Ising-type alloy [5,7] instead of a rotationally averaged alloy. In the latter case, the configuration average has to be performed over *all directions* of the local magnetic moments rather than by averaging over the *two orientations* ⇑ and ⇓.

Eventually, we obtain the mapping $T(c_{\Uparrow})$ by equating $\langle m \rangle(c_{\Uparrow})$ from the DLM calculations [Fig. 2(a)] and $\langle m \rangle(T; c_{\Uparrow})$ from the MC simulations (Fig. 4), which is shown as filled triangles in Fig. 5 and also displayed as top axis in Fig. 2. The mapping is monotonous but nonlinear.

As an application we show the $\langle m \rangle(T)$ curve for the 'optimal' (temperature-dependent) set of $\{J_{ij}(T)\}$ in Fig. 4 ('opt', large filled circles). It interpolates smoothly between the curve for $c_{\Uparrow} = 1.0$ at low temperatures and the curve for $c_{\Uparrow} = 0.5$ close to T_c. As a consequence, the critical exponent β is about 10% larger than that for $c_{\Uparrow} = 0.5$. The 'optimal' MC value of 0.349 is closer to the literature value of 0.365 [28] than those for $c_{\Uparrow} = 0.5$ (0.314) and $c_{\Uparrow} = 1.0$ (0.315). β was obtained by approximating $\langle m \rangle(T)$ by $(T_c - T)^{\beta}$ (dotted lines in Fig. 4), in which T_c has been fixed by the U_4 analysis [18,23].

3.2. Co

While the DLM approach works well for Fe, it fails for Ni. For example, the local magnetic moments vanish for paramagnetic Ni. Co has with one *d* electron more than Fe and one *d* electron less than Ni. Hence, it falls in-between Fe and Ni, which shows up as significantly reduced local moment for paramagnetic Co (about 0.80 μ_B) as compared to that of ferromagnetic Co (1.60 μ_B). These findings call for an improved DLM approach that, for example, takes into account short-range order.

Regardless of these shortcomings we present in Fig. 6 the major outcomes of our computations for hcp Co. In contrast to Fe (Fig. 5), T_c increases with $c_{\Uparrow}$ [filled circles in Fig. 6(b)] which is in line with the reduced local magnetic moments and the slightly

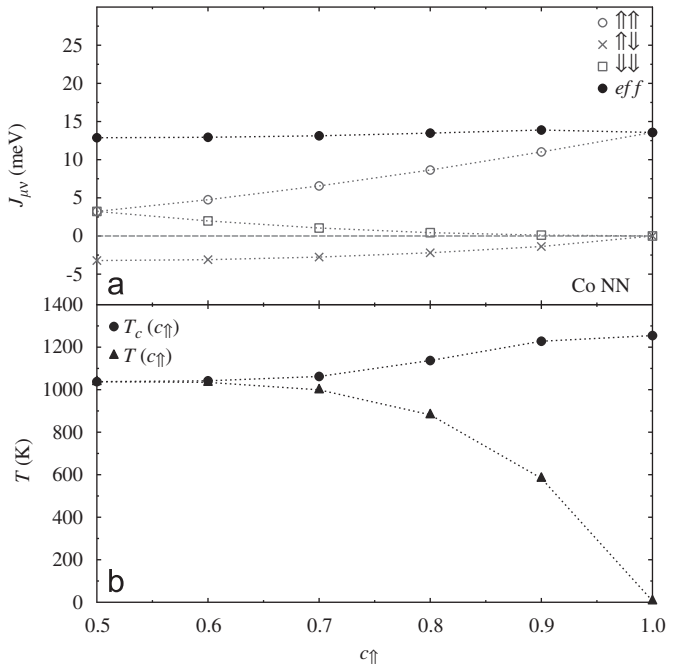

Fig. 6. Temperature-dependent exchange coupling in bulk Co. (a) Nearest-neighbor exchange coupling constants $J_{\Uparrow\Uparrow}$ (empty circles), $J_{\Uparrow\Downarrow}$ (crosses), $J_{\Downarrow\Downarrow}$ (empty squares) are depicted versus concentration $c_\Uparrow$. The effective constant J_{eff} (filled circles) increases slightly with $c_\Uparrow$. (b) Critical temperature and temperature mapping. T_c is displayed versus concentration $c_\Uparrow$ (filled circles), while the temperature mapping $T(c_\Uparrow)$ is represented by filled triangles. Lines serve as guides to the eye.

increasing effective exchange coupling constant [Fig. 6(a)]. Consequently, T_c is closest to the experimental value of 1388 K for $c_\Uparrow = 1$ (1255 K).

The general shape of the temperature-concentration mapping for Co [filled triangles in Fig. 6(b)] agrees with that for Fe (Fig. 5). But while the curve for Fe is almost linear for $c_\Uparrow > 0.7$, the Co mapping is bent downward. We attribute this observation to the almost constant J_{eff} of Co [filled circles in Fig. 6(a)] in contrast to the decreasing ones of Fe [filled circles in Fig. 2(b)].

4. Concluding remarks

In this paper, we propose a procedure to improve on the first-principles basis of Heisenberg exchange coupling constants. Since (i) the computation of Heisenberg exchange coupling constants within the DLM formalism is straightforward in any electronic-structure computer code that is based on Green functions and (ii) Monte Carlo simulations of the classical Heisenberg model can be regarded as standard as well, we see many applications for refined J_{ij}, in particular in magnetization dynamics calculations based on the Landau–Lifshitz–Gilbert equation. There, the Gilbert damping constant depends on temperature [29]; further, thermal fluctuations are modeled as random magnetic fields [1,2]. Hence, it is obvious to use temperature-dependent exchange coupling constants in the spin Hamiltonian as well. To complement the Heisenberg model, one could also include the temperature dependence of the magnetocrystalline anisotropy [30].

The purpose of the present study is to introduce the basic idea of the approach and to present a few applications. It also suggests paths for improvement: we expect that taking into account short-range order in the DLM calculations could result in better critical temperatures, which would also amend the temperature-concentration mapping. Rotational averaging rather than Ising-type averaging could improve the results as well; note that rotational averaging is a necessary ingredient if spin–orbit coupling should be accounted for, e.g. the Dzyaloshinskii–Moriya interaction [10,31–33].

The Dzyaloshinskii–Moriya interaction can lead to noncollinear magnetism in non-centrosymmetric systems, for example in ultrathin films on a substrate (e.g. Fe/Ir(111) [34]). The noncollinear magnetic structure gives rise to a 'magnetic lattice' constant which is determined by the ratios of Heisenberg exchange, magnetocrystalline anisotropy, and strength of the Dzyaloshinskii–Moriya interaction. Both may differ in their distance dependence and in their temperature dependence. Thus, one might speculate that a noncollinear structure, and hence its magnetic lattice constant, can vary significantly with temperature.

Acknowledgments

This work is supported by the *Sonderforschungsbereich*762 'Functional Oxide Interfaces'. DB is a member of the International Max Planck Research School on Science and Technology of Nanostructures, Halle, Germany. We appreciate helpful discussions with A. Marmodoro.

References

[1] B. Skubic, J. Hellsvik, L. Nordström, O. Eriksson, A method for atomistic spin dynamics simulations: implementation and examples, Journal of Physics: Condensed Matter 20 (2008) 315203.
[2] D. Böttcher, A. Ernst, J. Henk, Atomistic magnetization dynamics in nanostructures based on first principles calculations: application to Co nanoislands on Cu(111), Journal of Physics: Condensed Matter 23 (2011) 296003.
[3] A.I. Liechtenstein, M.I. Katsnelson, V.P. Antropov, V.A. Gubanov, Local spin density functional approach to the theory of exchange interactions in ferromagnetic metals and alloys, Journal of Magnetism and Magnetic 67 (1987) 65.
[4] J. Staunton, B.L. Gyorffy, A.J. Pindor, G.M. Stocks, H. Winter, The "Disordered local moment" picture of itinerant magnetism at finite temperatures, Journal of Magnetism and Magnetic 45 (1984) 15–22.
[5] B.L. Gyorffy, A.J. Pindor, J. Staunton, G.M. Stocks, H. Winter, A first-principles theory of ferromagnetic phase transitions in metals, Journal of Physics F: Metal Physics 15 (6) (1985) 1337–1386.
[6] S.S.A. Razee, J.B. Staunton, L. Szunyogh, B.L. Györffy, Local moments and magnetic correlations above the Curie temperature in thin films on and embedded in nonmagnetic substrates: Fe/Cu(100), Co/Cu(100), and Fe/W(100), Physical Review B 66 (2002) 094415.
[7] A.J. Pindor, J. Staunton, G.M. Stocks, H. Winter, Disordered local moment state of magnetic transition metals: a self-consistent KKR CPA calculation, Journal of Physics F: Metal Physics 13 (1983) 979.
[8] A.V. Ruban, S. Khmelevskyi, P. Mohn, B. Johansson, Temperature-induced longitudinal spin fluctuations in Fe and Ni, Physical Review B 75 (2007) 054402.
[9] V. Drchal, J. Kudrnovský, P. Bruno, P.H. Dederichs, P. Weinberger, The combined effect of temperature and disorder on interlayer exchange coupling in magnetic multilayers, Philosophical Magazine B 78 (1998) 571.
[10] A. Buruzs, Temperature Dependent Magnetic Properties of Thin Films and Bulk Ferromagnets: An Implementation of the Disordered Local Moment Scheme, PhD Thesis, Fakultät für Physik, Technische Universität Wien, Vienna, 2008.
[11] J. Zabloudil, R. Hammerling, L. Szunyogh, P. Weinberger (Eds.), Electron Scattering in Solid Matter, Springer, Berlin, 2005.
[12] J.P. Perdew, Y. Wang, Accurate and simple analytic representation of the electron-gas correlation energy, Physical Review B 45 (1992) 13244.
[13] P. Soven, Coherent-potential model of substitutional disordered alloys, Physical Review 156 (1967) 809.
[14] B.L. Gyorffy, Coherent-potential approximation for a nonoverlapping-muffin-tin-potential model of random substitutional alloys, Physical Review B 5 (1972) 2382.
[15] J.S. Faulkner, G.M. Stocks, Calculating properties with the coherent-potential approximation, Physical Review B 21 (1980) 3222.
[16] P.J. Durham, B.L. Gyorffy, A.J. Pindor, On the fundamental equations of the Korringa-Kohn-Rostoker (KKR) version of the coherent potential approximation (CPA), Journal of Physics F: Metal Physics 10 (1980) 661.

[17] N. Metropolis, A.W. Rosenbluth, M.N. Rosenbluth, E. Teller, Equation of state calculations by fast computing machines, Journal of Chemical Physics 21 (1953) 1087.
[18] K. Binder, Applications of Monte Carlo methods to statistical physics, Reports on Progress in Physics 60 (1997) 487.
[19] A.L. Wysocki, R.F. Sabirianov, M. van Schilfgaarde, K.D. Belashchenko, First-principles analysis of spin-disorder resistivity of Fe and Ni, Physical Review B 80 (2009) 224423.
[20] A. Sakuma, First principles study on the exchange constants of the 3d transition metals, Journal of Physical Society of Japan 68 (1998) 620.
[21] M. van Schilfgaarde, V.P. Antropov, First-principles exchange interactions in Fe, Ni, and Co, Journal of Applied Physics 85 (1999) 4827.
[22] I. Turek, J. Kudrnovský, V. Drchal, P. Bruno, Exchange interactions, spin waves, and transition temperatures in itinerant magnets, Philosophical Magazine 86 (2006) 1713.
[23] K. Binder, D.W. Heermann, Monte Carlo Simulation in Statistical Physics: An Introduction, third ed, Springer, Berlin, 1997.
[24] K.S. Chana, J.H. Samson, M.U. Luchini, V. Heine, Magnetic short-range order in iron above T_c? Statistical mechanics with many-atom interactions, Journal of Physics: Condensed Matter 3 (1991) 6455.
[25] D. Reiser, J. Henk, H. Gollisch, R. Feder, Theory of temperature-dependent electronic structure and photoemission of ultrathin ferromagnetic films, Solid State Communications 93 (1995) 231.
[26] P. Weinberger, R. Dirl, A.M. Boring, A. Gonis, A.J. Freeman, Fully relativistic Korringa-Kohn-Rostoker coherent-potential-approximation embedded-cluster-method evaluation of short-range-order effects in substitutional alloys containing heavy elements, Physical Review B 37 (1988) 1383.
[27] I.A. Abrikosov, A.M.N. Niklasson, S.I. Simak, B. Johansson, A.V. Ruban, H.L. Skriver, Order-N Green's function technique for local environment effects in alloys, Physical Review Letters 76 (1996) 4203.
[28] M. Getzlaff, Fundamentals of Magnetism, Springer, Berlin, 2008.
[29] H. Ebert, S. Mankovsky, D. Ködderitzsch, P.J. Kelly, Ab-initio calculation of the Gilbert damping parameter via linear response formalism, arxiv:1102.4551v1 [cond-mat.mtrl-sci] (2011).
[30] A. Buruzs, P. Weinberger, L. Szunyogh, L. Udvardi, P.I. Chleboun, A.M. Fischer, J.B. Staunton, Ab initio theory of temperature dependence of magnetic anisotropy in layered systems: applications to thin Co films on Cu(100), Physical Review B 76 (6) (2007) 064417.
[31] I. Dzyaloshinsky, A thermodynamic theory of "weak" ferromagnetism of antiferromagnetics, Journal of Physics and Chemistry of Solids 4 (4) (1958) 241. doi:10.1016/0022-3697(58)90076-3.
[32] T. Moriya, Anisotropic superexchange interaction and weak ferromagnetism, Physical Review 120 (1960) 1.
[33] L. Udvardi, L. Szunyogh, K. Palotás, P. Weinberger, First-principles relativistic study of spin waves in thin magnetic films, Physical Review B 68 (2003) 104436.
[34] K. von Bergmann, S. Heinze, M. Bode, G. Bihlmayer, S. Blügel, R. Wiesendanger, Complex magnetism of Fe monolayer on Ir(111), New Journal of Physics 9 (2007) 396.